Proposal and Validation of a Series Hybrid System Using a DC-Input Direct Electric-Power Converter D-EPC

Hiroki Matsuno[1*], Hiromu Akiyama[1], Kantaro Yoshimoto[1] and Tomoki Yokoyama[1]
[1] Department of Robotics and Mechatronics, Tokyo Denki University, Tokyo, Japan
*E-mail: 22fmr41(a)ms.dendai.ac.jp

***Abstract*-- A novel hybrid system using DC-input direct electric-power converter (D-EPC) has been proposed. D-EPC is an inverter capable of controlling the distribution of power from two sources. In this paper, the power distribution control of D-EPC achieves the voltage boost for series hybrid system without a boost chopper. The voltage of the smoothing capacitor is controlled at a constant level using the power distribution control of D-EPC to maintain the motor drive voltage regardless of load variations. The effectiveness of the proposed hybrid system was verified by simulation and the prototype D-EPC circuit.**

***Index Terms*-- power conversion, power control, boost control, hybrid vehicle**

I. Introduction

The hybrid system with a boost chopper shown in Fig.1 [1] is widely used in current hybrid electric vehicles, but the loss caused by the boost chopper and the increase in mass and volume due to the boost inductor inside the boost chopper are issues to be addressed. This paper proposes a hybrid system without a boost chopper by using DC-input direct electric-power converter (D-EPC) [2] ~ [6]. Figure 2 shows a hybrid system using the D-EPC. D-EPC has been proposed as inverter two DC power sources inputs. Although hybrid systems using the D-EPC require more semiconductor switches than conventional hybrid systems, they are still expected to be more efficient, lightweight, and compact because of the elimination of the boost inductor. Furthermore, power semiconductors technology is evolving faster than that of boost inductors, so they are expected to become even more efficient and lightweight in the future. The circuit topology of D-EPC with DC Power Sources Connected in Series itself is same as a 3-level-inverter. For 3-level-inveters, the neutral point potential is controlled by the neutral current[7]~[12]. It could be considered that this neutral current control and the neutral point potential control could be used for power control of unbalanced voltage sources which are connected with different power sources. However, D-EPC control activates each inverter connected with a power source in each carrier cycle using the distributed phase voltage commands which can be calculated easily by multiplying the power distribution ratio as command value and the phase voltage command. This power distribution of D-EPC has the advantage as quick response of power control for DC power sources. Because the power is distributed by phase voltage command by each carrier cycle. These features of D-EPC control are different from the 3-level-inverter control using neutral point potential. In the hybrid system with D-EPC, the battery is connected as power

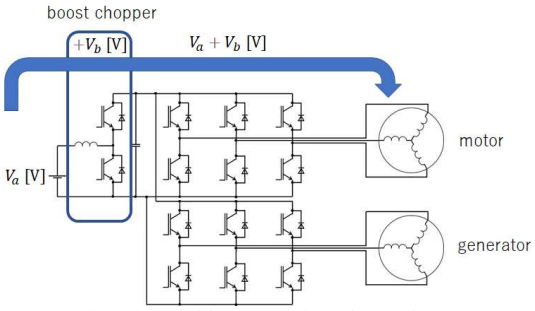

Fig. 1. Hybrid system using a boost chopper.

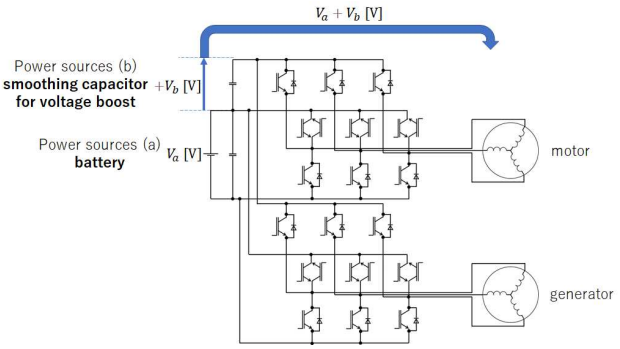

Fig. 2. Hybrid system using D-EPC.

source (a), and power source (b) is like a pole without a power supply only connected the smoothing capacitor. In order to use these series voltages to drive the motor, so the smoothing capacitor voltage as (b) is boosted by controlling the power distribution as a unique function of D-EPC.

A. Power distribution control by D-EPC

Figure 3 shows the power sources and one leg circuit diagram of D-EPC. In the power distribution control of the D-EPC, the ratio of the output voltage distribution to these two power sources is considered. This is achieved by the given power distribution command value and the dq-axis current command value of the motor. The phase voltage

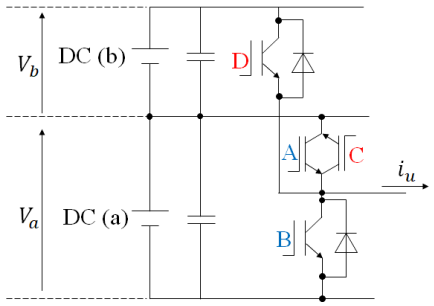

Fig. 3. Power sources and one leg circuit diagram of D-EPC.

©2023 KIPE

command values for each of the power source are considered by calculating three-phase voltage command values using vector control from the dq-axis current command values and multiplying the calculated phase voltage command values using the distribution command values. Furthermore, for Pulse Width Modulation (PWM) signal generation by triangular wave comparison, the scale of the phase voltage command values of each power source is converted to the modulation ratio. The modulation ratio of the u-phase of power source (a) m_{ua} is obtained by (1), where V_a [V] is the power source (a) voltage, γ_a is the power distribution command value, and v_u^* [V] is the u-phase voltage command value.

$$m_{ua} = 2\gamma_a \frac{v_u^*}{V_a} \tag{1}$$

Equation (2) shows the relationship between the distribution command value γ_a for power source (a) and the distribution command value γ_b for power source (b). Considering that output voltage is realized by two power sources, the sum of the distribution command values for each power source is equal to one.

$$\gamma_a + \gamma_b = 1 \tag{2}$$

Equation (3) shows how to derive the modulation ratio of the u-phase of power source (b) m_{ub}. It is derived using the power source (a) distribution command value based on the relationship of the power distribution ratio in D-EPC shown in (2).

$$m_{ub} = 2(1-\gamma_a)\frac{v_u^*}{V_b} \tag{3}$$

The v-phase and w-phase modulation ratio of each power source are also obtained by the same manner as (3). Figure 4 shows the relationship between the modulation ratio and the triangular wave. To avoid the short circuit by bi-directional switches, offsets m_{oa} and m_{ob} are added to the modulation ratio m_{ua} and m_{ub} of each power source, respectively. The offset values m_{oa} and m_{ob} are obtained from the time distribution of the PWM cycle according to the power distribution ratio.

Equation (4) shows the how to derive the offset value for the modulation ratio of power source (a). The offset of power source (a) is considered the offset reference as the upper limit of the triangular wave, and subtracted by the time distribution ratio according to the power distribution ratio of power source (a) shown in the second term of (4).

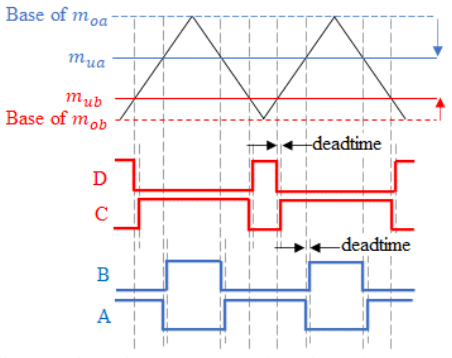

Fig. 4. Triangular wave comparison for series D-EPC

$$m_{oa} = 1 - \frac{\left|\frac{\gamma_a}{V_a}\right|}{\left|\frac{\gamma_a}{V_a}\right| + \left|\frac{\gamma_b}{V_b}\right|} \tag{4}$$

Equation (5) shows how to derive the offset value for the modulation ratio of power source (b). The offset of power source (b) is considered the offset reference as the lower limit of the triangular wave, and added the time distribution ratio shown in the first term of (5) which depends on the power distribution ratio of power source (b).

$$m_{ob} = \frac{\left|\frac{\gamma_b}{V_b}\right|}{\left|\frac{\gamma_a}{V_a}\right| + \left|\frac{\gamma_b}{V_b}\right|} - 1 \tag{5}$$

From the above calculation, the final output u-phase modulation ratio m_{uac} of power source (a) is shown in (6). The final output u-phase modulation ratio m_{ubc} of power source (b), obtained by the same manner, is shown in (7).

$$m_{uac} = m_{ua} + m_{oa} \tag{6}$$

$$m_{ubc} = m_{ub} + m_{ob} \tag{7}$$

The PWM signal is generated by comparing these final outputs with a triangular wave, and the PWM signal realizes switching of the D-EPC according to the modulation rates to achieve arbitrary power distribution.

II. Hybrid System Using The Power Distribution Control Of The D-EPC

A. Boosting control using power distribution control

The voltage boosting control in the hybrid system controls the distribution ratio of generated power from the generator to the two inputs shown in Fig. 3 using power distribution control. The controller determines the distribution command value by two-degree-of-freedom control: feedforward control based on the power consumption of the capacitor (b) by the motor drive and feedback control based on the deviation between the target voltage value and actual voltage value of the capacitor (b). Figure 5 shows the control block diagram of the voltage boost control. In feedforward control, the distribution ratio γ_{FF} is considered as the ratio of the capacitor (b) power consumption P_c [W] by the drive motor to the power generated P_e [W] by the generator. The capacitor (b) power consumption is derived from the power distribution ratio γ_{drive} on the drive side D-EPC and the power of motor drive P_{drive} [W]. Equation (8) shows how to derive the power of motor drive P_{drive} [W] at motor side. Where R [Ω] is the winding resistance of the Permanent Magnet Synchronous Motor (PMSM), i_d [A] is the d-axis current command value, i_q [A] is the q-axis current command value, ω [rad/s] is the electric angular velocity, ψ [Wb] is the magnetic flux linkage, L_d [H] is the d-axis inductance, L_q [H] is the q-axis inductance.

$$P_{drive} = R\left(i_d^2 + i_q^2\right) + \omega i_q\left\{\psi + i_d\left(L_d - L_q\right)\right\} \tag{8}$$

The power consumption of the smoothing capacitor (b) P_c [W] is derived as the product of the power of motor drive P_{drive} [W] shown in (8) and the power distribution

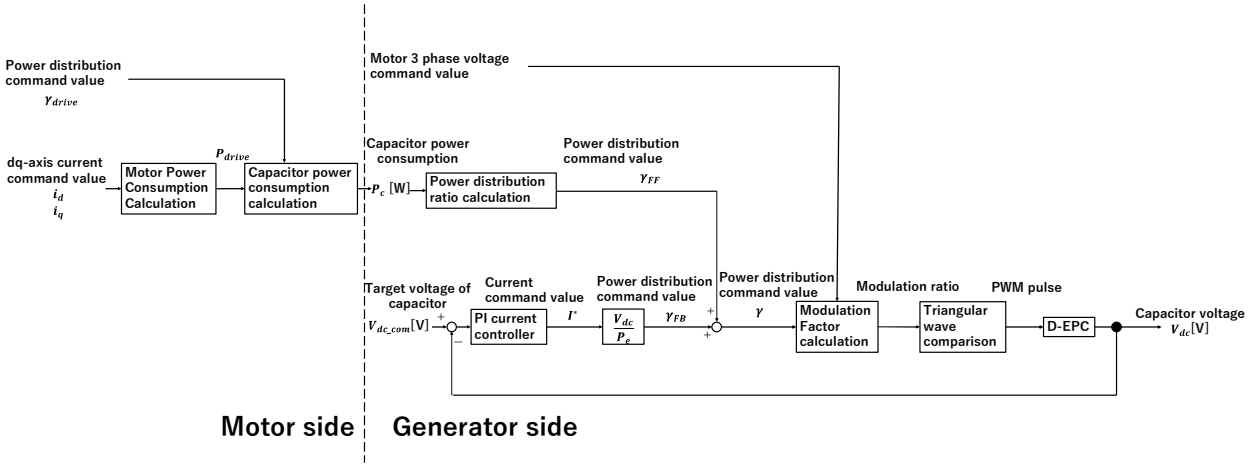

Fig. 5. Control block diagram for boosting control for hybrid system using D-EPC

ratio γ_{drive} for the smoothing capacitor (b). Therefore, the distribution ratio γ_{FF} at the generator side D-EPC is derived by (9). Where P_e [W] is the generated power by the generator. The generator power P_e [W] is derived in the same manner as in (8).

$$\gamma_{FF} = \frac{P_{drive} \cdot \gamma_{drive}}{P_e} = \frac{P_c}{P_e} \tag{9}$$

In feedback control, PI current controller reacts to the error between the target voltage V_{dc_com} [V] and the actual voltage V_{dc} [V]. The target voltage V_{dc_com} [V] is the capacitor (b) voltage value required to boost the voltage at the drive motor side. In this paper, the PI gain is designed by considering the plant model as an RC parallel circuit in which the output voltage of capacitor V_{dc} [V] has a primary delay with input current I^* [A] shown in Fig. 6. Equation (10), (11) shows the transfer function $P(s)$ of the modeled RC parallel circuit. Where C [F] is the capacitance of the boost capacitor (b) used and r [Ω] gives the virtual parallel resistance as a factor indicating loss.

$$V_{dc} = \frac{r}{rCs+1} I^* = P(s) I^* \tag{10}$$

$$P(s) = \frac{r}{rCs+1} \tag{11}$$

Equation (12) shows the closed-loop transfer function $G_{pi}(s)$ of the PI control system. Where $C_{pi}(s)$ is the transfer function of the PI current controller and $P(s)$ is the transfer function of the plant shown in (11). Equation (13) also shows the transfer function $G(s)$ of the first-order delay system when the cutoff frequency is ω_c [rad/s].

$$G_{pi}(s) = \frac{C_{pi}(s)P(s)}{1+C_{pi}(s)P(s)} \tag{12}$$

$$G(s) = \frac{\omega_c}{s+\omega_c} \tag{13}$$

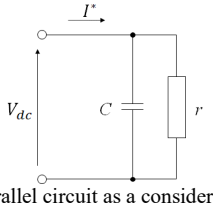

Fig. 6. RC parallel circuit as a consideration model for boosting control.

Design the PI gain by solving for $C_{pi}(s)$ so that (12) and (13) are equivalent. Equation (14) shows the result of solving for $C_{pi}(s)$ based on (11), (12), and (13).

$$C_{pi}(s) = \omega_c C + \omega_c \frac{1}{r} \cdot \frac{1}{s} \tag{14}$$

From the (14), the proportional gain k_p and integral gain k_i become equations (15) and (16), respectively.

$$k_p = \omega_c C \tag{15}$$

$$k_i = \omega_c \frac{1}{r} \tag{16}$$

Equation (17) shows the distribution ratio γ_{FB} by feedback control. To apply the operating amount of current I^* [A] calculated by the PI control described above to D-EPC, it is converted from the boost capacitor (b) voltage V_{dc} [V] and the generated power P_e [W] to the allocation command value γ_{FB}.

$$\gamma_{FB} = \frac{V_{dc} \cdot I^*}{P_e} \tag{17}$$

From the above, the final distribution command value γ, which consists of feedback control designed for transient response and feedforward control to compensate for disturbances caused by motor drive, is obtained by (18).

$$\gamma = \gamma_{FF} + \gamma_{FB} \tag{18}$$

B. Verification of series hybrid system using D-EPC by simulation

To confirm the validity of the hybrid system using D-EPC, the simulation validation was conducted. Table 1. shows the parameters used in the verification by the simulation. In the simulations, the element r [Ω], which represents the loss, was set to a value that would result in a loss of 10% of the generated power, assuming an efficiency of 90%. The target smoothing capacitor (b) voltage was set as 500 [V], the generator was controlled to generate power at 1000 [min^{-1}], and the motor was driven at 1000 [min^{-1}]. In addition, the same Permanent Magnet Synchronous Motor (PMSM) model was used as the generator and drive motor. Figure 7 shows the voltage of the smoothing capacitor (b) corresponding to the power

source (b). It was confirmed that the smoothing capacitor (b) voltage could be boosted to the target voltage regardless of load fluctuations caused by changes in the distribution ratio on the motor drive side. At the same time, verified the distribution of motor drive power in the hybrid system using D-EPC. Figure 8 shows the relationship between the power for motor drive of battery side corresponding to the power source (a) and the power for motor drive of smoothing capacitor (b) side corresponding to the power source (b). From 0.2 [s] to 1.2 [s], the D-EPC distribution command value on the drive side was varied from 0.0 to 1.0 by 0.1 every 0.1 [s]. It was confirmed that the motor can be driven while achieving the desired distribution ratio according to the command value. These results confirm the effectiveness of the hybrid system using D-EPC, which does not require a boost chopper.

Table 1. Parameters used for simulation.

Parameter [unit]	Symbol	Value
D-axis current command value [A] (Drive side)	$i_{d\_drive}^{*}$	-50
Q-axis current command value [A] (Drive side)	$i_{q\_drive}^{*}$	50
D-axis current command value [A] (Generator side)	$i_{d\_gene}^{*}$	-100
Q-axis current command value [A] (Generator side)	$i_{q\_gene}^{*}$	-100
Capacitor voltage command [V]	v_c	500
Motor revolution speed [min^{-1}] (Drive side)	—	1000
Motor revolution speed [min^{-1}] (Generator side)	—	1000
Number of poles pairs (common)	—	4
Magnetic flux [mWb] (common)	ψ	78
Stator winding resistance [mΩ] (common)	R	10
D-axis inductance [μH] (common)	L_d	200
Q-axis inductance [μH] (common)	L_q	300
Smoothing capacitor [mF]	C	1
Virtual parallel resistance [Ω]	r	625
cutoff frequency [rad/s]	ω_c	1000

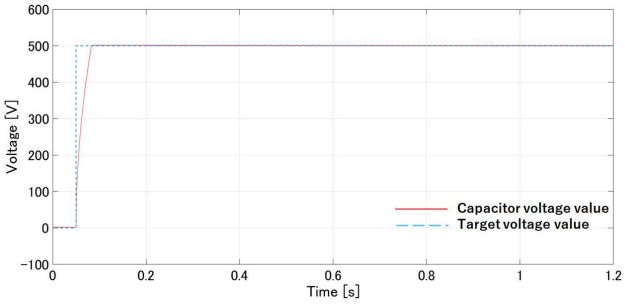

Fig. 7. Smoothing capacitor voltage in the hybrid system using D-EPC (simulation).

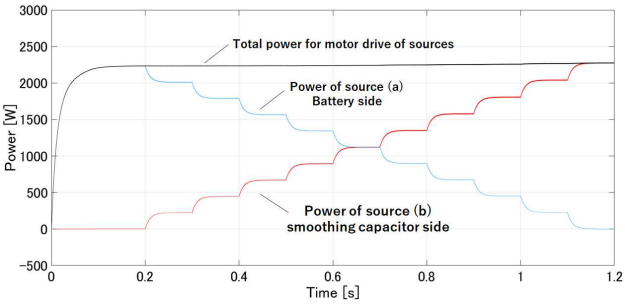

Fig. 8. Power distribution in the hybrid system using D-EPC (simulation).

C. *Verification of hybrid system using D-EPC by the prototype D-EPC circuit*

To confirm the validity of the new hybrid system using D-EPC, also verified the actual system with a prototype D-EPC circuit and motor bench. Figure 9 shows an actual machine configuration. A motor bench consisting of a

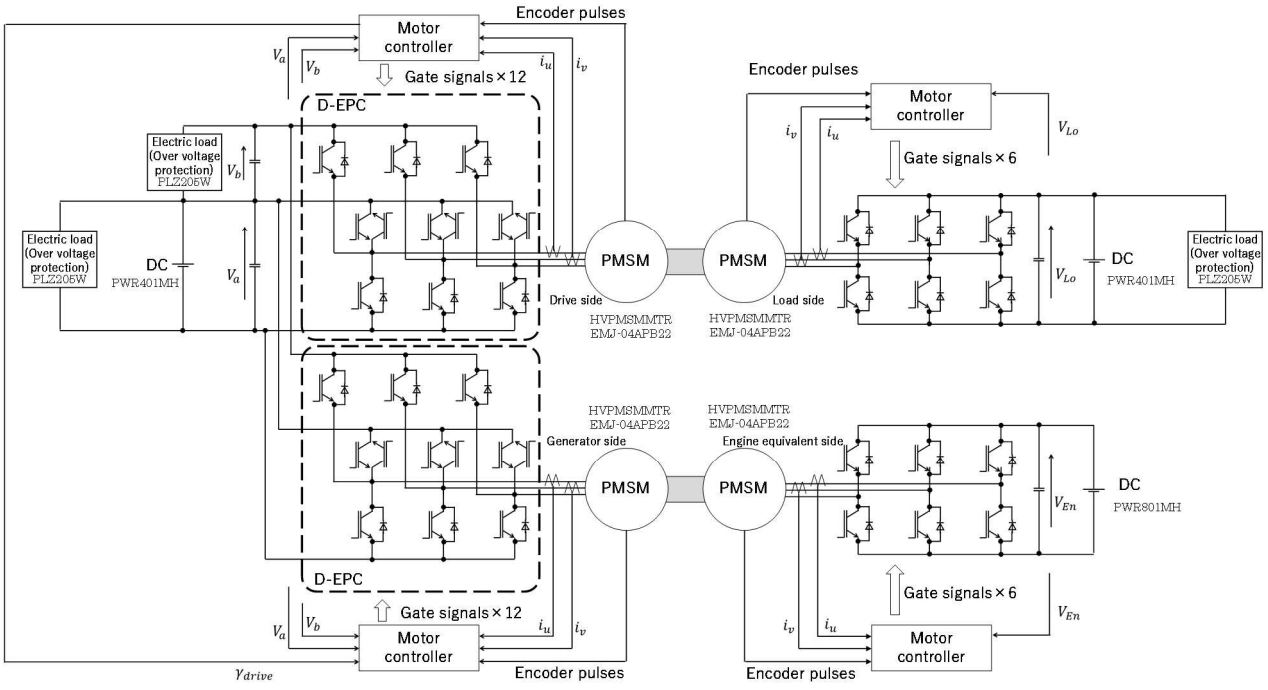

Fig. 9. Experimental configuration using a prototype D-EPC circuit

PMSM “EMJ-04APB22” with a rated output of 400 [W] is used as the drive motor, load motor, engine equivalent motor, and generator [13]. The load motor and engine-equivalent motor are driven by a three-phase inverter for speed control. The main circuit of the prototype D-EPC is using Fuji Electric's “12MBI50VN-120-50”, which has Reverse Blocking Insulated Gate Bipolar Transistors (RB-IGBTs) [14] for bi-directional switches. In order to perform feed-forward control, the controller on the drive side sends the value of the power consumption of the smoothing capacitor (b) P_c [W] to the controller on the generator side using the Serial Communications Interface (SCI). Table 2. shows the parameters used in the verification by the prototype D-EPC circuit. In the verification by the actual machine, the element r [Ω], which represents the loss, was set to a value that would result in a loss of 20% of the generated power, assuming an efficiency of 80%. The target smoothing capacitor (b) voltage was set as 50 [V], the generator was controlled to generate power at 1000 [min^{-1}], and the motor was driven at 500 [min^{-1}]. As with verification by simulation, generator side and drive side use the motor bench with the same parameters. Smoothing capacitor (b) with a capacitance of 1 [mF] were connected in series for both inputs. Figure 10 shows the voltage of the smoothing capacitor (b) corresponding to the power source (b). It was confirmed that the smoothing capacitor (b) voltage could be boosted to the target voltage regardless of load fluctuations caused by changes in the distribution ratio on the motor drive side. As in the simulation, verified the distribution of motor drive power in the hybrid system using D-EPC. Figure 11 shows the relationship between the power for motor drive of battery corresponding to the power source (a) side and the power for motor drive of smoothing capacitor (b) corresponding to the power source (b) side. In the verification by the prototype D-EPC circuit, after confirming the capacitor (b) voltage boost, the D-EPC distribution command value on the drive side was varied from 0.0 to 1.0 by 0.1 every 2.0 [s]. Although errors occurred unlike the simulation results,

Table 2. Parameters used for actual device verification.

Parameter [unit]	Symbol	Value
D-axis current command value [A] (Drive side)	$i_{d\_drive}{}^*$	0
Q-axis current command value [A] (Drive side)	$i_{q\_drive}{}^*$	2
D-axis current command value [A] (Generator side)	$i_{d\_gene}{}^*$	0
Q-axis current command value [A] (Generator side)	$i_{q\_gene}{}^*$	-3
Capacitor voltage command [V]	v_c	50
Motor revolution speed [min^{-1}] (Drive side)	—	500
Motor revolution speed [min^{-1}] (Generator side)	—	1000
Number of poles pairs (common)	—	4
Magnetic flux [mWb] (common)	ψ	61.5
Stator winding resistance [mΩ] (common)	R	2.7
D-axis inductance [μH] (common)	L_d	8.5
Q-axis inductance [μH] (common)	L_q	8.5
Smoothing capacitor [mF]	C	1
Virtual parallel resistance [Ω]	r	250
cutoff frequency [rad/s]	ω_c	500

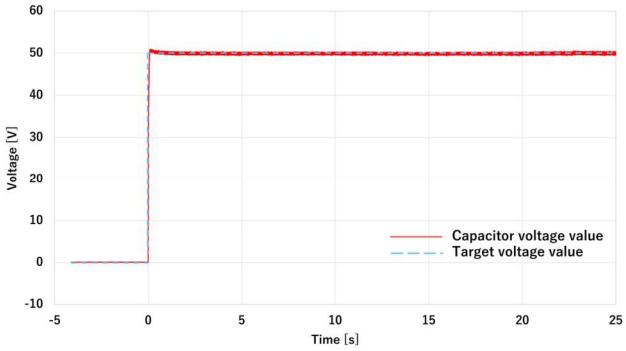

Fig. 10. Smoothing capacitor voltage in the hybrid system using D-EPC (experimental result).

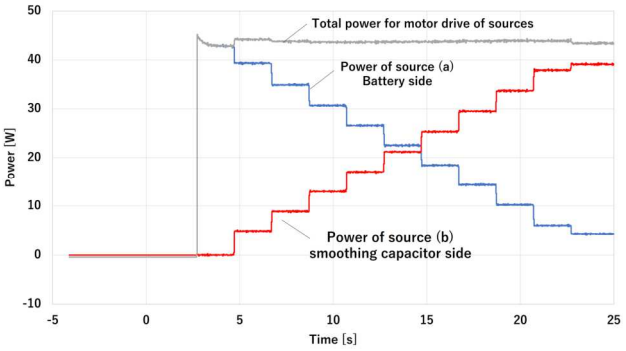

Fig. 11. Power distribution in the hybrid system using D-EPC (experimental result).

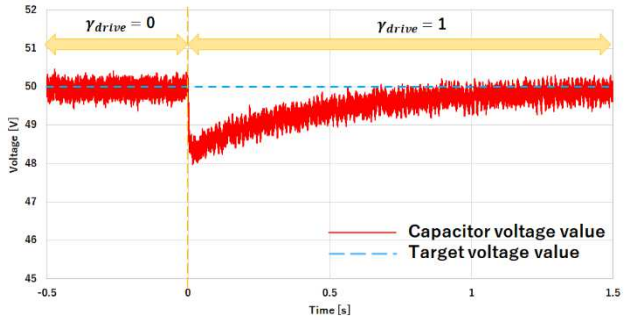

Fig. 12. Capacitor voltage at power consumption (Feedback control only).

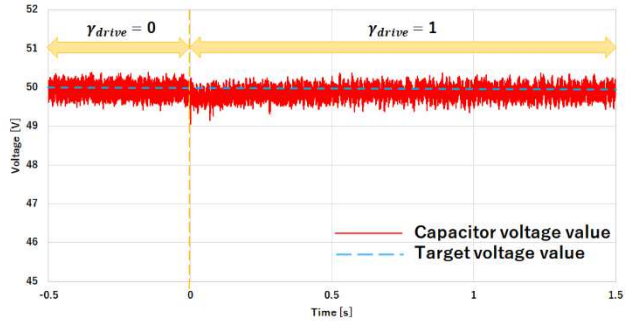

Fig. 13. Capacitor voltage at power consumption (Two-degree-of-freedom control).

the motor can be driven while achieving the desired distribution ratio according to the command value.

As the next experiment, to verify the effectiveness of the two-degree-of-freedom control against voltage drop due to motor drive, after confirming the voltage boost, the motor

was driven with only the smoothing capacitor (b) and verified the voltage fluctuation. Figure 12 shows the measured voltage of smoothing capacitor (b) for voltage boost controlled by feedback control, and Fig. 13 shows that by two-degree-of-freedom control. It was confirmed that the two-degree-of-freedom control was able to compensate for the voltage drop associated with the motor drive.

These results confirm the effectiveness of the hybrid system with D-EPC, which does not require a boost chopper, as verified by actual equipment.

III. CONCLUSIONS

This paper proposes the novel hybrid system using D-EPC as a hybrid system without a boost chopper. Simulation verification results show that the system can drive the motor with the power distribution as commanded and boost the voltage of the smoothing capacitor (b) regardless of the disturbance caused by the motor drive, and that the system functions as a hybrid system. In addition, the results of the verification using the prototype D-EPC circuit showed that the distribution was success, and the voltage of the smoothing capacitor (b) was boosted regardless of disturbances caused by the motor drive, and the hybrid system was confirmed to function in the verification actual device too. As for the robustness against disturbances caused by motor drive, it was confirmed that the voltage drop can be compensated by the voltage boosting control with two degrees of freedom control in the results of the verification using the prototype D-EPC circuit. In the results of the verification using the prototype D-EPC circuit, unlike the simulation results, there were errors in the power distribution during motor drive. Causes of errors and countermeasures will be investigated in the future.

ACKNOWLEDGMENT

This work is supported partly by a research grant of JDC Foundation Inc.

REFERENCES

[1] M. Okamura and T. Takaoka, “The Evolution of Electric Components in Prius”, IEEJ Journal of Industry Applications Vol.11, No.1, pp.1-6 (2022)

[2] K. Yoshimoto, S. Satou, K. Maikawa, and K. Takahashi, “Multiple-DC-Inputs Direct Electric Power Converter D-EPC with DC Power Sources Connected in Series”, T.IEE Japan, Vol.132-D, No.3, pp.445-451 (2012)

[3] K. Yoshimoto, S. Satou, and K. Maikawa, “A Novel Multiple DC-Inputs Direct Electric-Power Converter”, SAE Int. J. Passeng. Cars – Electron. Electr. Syst. 2 (1), pp.94-100 (2009)

[4] K. Yoshimoto, K. Maikawa, and S. Satou, “Novel Multiple DC-inputs Direct Electric-Power Converter”, EPE Journal Vol.20, No.2, pp.36-41 (2010)

[5] K. Yoshimoto, “Multiple-DC-Inputs Direct Electric Power Converter D-EPC Using Multiple Input Leg Reduction Topology and its Control”, IEEJ Journal of Industry Applications, Vol.9, No.3, pp.298-304 (2020)

[6] H. Akiyama, H. Matsuno, K. Yoshimoto and T. Yokoyama, “A Novel Charging Control for D-EPC with DC Power Sources Connected in Series”, IEEJ Journal of Industry Applications, https://doi.org/10.1541/ieejjia.22007921

[7] S. Ogasawara, H. Akagi, “Analysis of variation of neutral point potential in neutral-point-clamped voltage source PWM inverters”, IEEE Industry Applications Conference 28th IAS Annual Meeting, pp.965-970 (1993)

[8] Y. Park, S. -K. Sul, C. -H. Lim, W. -C. Kim and S. -H. Lee, “Asymmetric Control of DC-Link Voltages for Separate MPPTs in Three-Level Inverters”, IEEE Transactions on Power Electronics, Vol.28, No.6, pp.2760-2769 (2013)

[9] X. Wu, G. Tan, Z. Ye, G. Yao, Z. Liu and G. Liu, “Virtual-Space-Vector PWM for a Three-Level Neutral-Point-Clamped Inverter With Unbalanced DC-Links”, IEEE Transactions on Power Electronics, Vol.33, No.3, pp.2630-2642 (2018)

[10] K. Kondo, “Basic Study on An EDLC and DC voltage Hybrid Traction System with A Direct Converter”, Proc. International Power Electronics Conference (IPEC2010), pp.2147-2152 (2010)

[11] Y. Asano, Y. Ohno, S. Kurita, K. Kondo, K. Shinomiya, and K. Ishikawa, “Charge and Discharge Control to Save Regeneration Energy for Overhead Line and Energy Storage Device Hybrid Power Source Three Level Inverter”, IEEJ Trans. IA, Vol.137, No.5, pp.369-376 (2017)

[12] A. Shimada, Y. Noumi, K. Kondo, “Study on the Output Voltage Characteristics of the Unbalanced Input Voltage Three-Level Inverter”, IEEJ Trans. IA, Vol.134, No.1, pp.10-18 (2014)

[13] F. Mendoza-Mondragon, V. Manuel Hernandez-Guzman, and J. Rodriguez-Resendiz, “Robust Speed Control of Permanent Magnet Synchronous Motors Using Two-Degrees-of-Freedom Control”, IEEE Transactions on Industrial Electronics, Vol.65, No.8, pp.6099-6108 (2018)

[14] H. Nakazawa, D. Hongfei Lu, M. Ogino, T. Shirakawa, and Y. Takahashi, “Reverse-Blocking IGBTs with V-Groove Isolation Layer for Three-Level Power Converters”, IEEJ Journal of Industry Applications, Vol.2, No.6, pp.323-328 (2013)